

MIT Open Access Articles

Effect of ligand on thermal dissipation from gold nanorods

The MIT Faculty has made this article openly available. **Please share** how this access benefits you. Your story matters.

Citation: Alper, Joshua, and Kimberly Hamad-Schifferli. "Effect of Ligands on Thermal Dissipation from Gold Nanorods." *Langmuir* 26.6 (2010) : 3786-3789.

As Published: <http://dx.doi.org/10.1021/la904855s>

Publisher: American Chemical Society

Persistent URL: <http://hdl.handle.net/1721.1/65163>

Version: Author's final manuscript: final author's manuscript post peer review, without publisher's formatting or copy editing

Terms of Use: Article is made available in accordance with the publisher's policy and may be subject to US copyright law. Please refer to the publisher's site for terms of use.



Effect of ligand on thermal dissipation from gold nanorods

Joshua Alper¹ and Kimberly Hamad-Schifferli^{1,2}

¹Department of Mechanical Engineering, ²Department of Biological Engineering, Massachusetts Institute of Technology, Cambridge MA 02139 USA

AUTHOR EMAIL ADDRESS schiffer@mit.edu

RECEIVED DATE

CORRESPONDING AUTHOR FOOTNOTE schiffer@mit.edu

ABSTRACT Thermal interface conductance was measured for soluble gold nanorods (NRs) coated with mercaptocarboxylic acids (HS-(CH₂)_nCOOH, n = 5, 10, 15), thiolated polyethylene glycols (MW = 356, 1000, 5000), and HS-(CH₂)₁₅-COOH coated NRs further coated with alternating layers of poly(diallyldimethylammonium chloride) and poly(styrenesulfonate). Ferguson analysis determined ligand thickness. The thermal diffusion dominated regime of transient absorption spectra was fit to a continuum heat diffusion finite element model to obtain the thermal interface conductance, G , which varied with ligand chemistry but not molecule length. The results suggest that the ability to exclude water from the NR surface governs ligand G values.

Gold nanorods (NRs) are attractive for photothermal therapy,¹⁻³ drug delivery,⁴⁻⁶ therapeutic applications, and imaging.^{7, 8} These applications rely on laser irradiation of NRs at the longitudinal surface plasmon resonance (LSPR) wavelength. In particular, ultrafast pulsed laser irradiation specifically heats the NRs and not the surroundings, which makes this an interesting approach for triggered drug delivery.⁹⁻¹¹ Characterization of thermal dissipation is critical for applications in which NRs have a payload for release, especially for thermally sensitive molecules such as proteins and DNA.^{6, 12} Previous work showed that thermal dissipation is strongly influenced by the ligand density of hexadecyltrimethylammonium bromide (CTAB) coated NRs. As the density increased, the thermal interface conductance, G , decreased.¹³ However, utilizing NRs in biological applications often requires surface chemistry modification. Surface ligand type and length are commonly changed to meet biocompatibility and stability requirements¹⁴⁻¹⁶, so understanding how the ligand type and length affects thermal dissipation from the particle is important.

Here we use transient absorption spectroscopy to measure thermal dissipation¹⁷⁻¹⁹ from photoexcited gold nanorods that are functionalized with several different ligands²⁰, employing molecules that are popular for biological applications: mercaptocarboxylic acids (MCA), thiolated polyethylene glycol (PEG), and polyelectrolyte layers assembled by layer-by-layer approaches. By fitting to a continuum heat diffusion model, we obtain values for the thermal interface conductance, G . NR ligand chemistry strongly influences thermal dissipation and G , while ligand length has no effect above a certain length. These results suggest that the ability of a ligand to keep water from the NR surface is a key factor in regulating the thermal interface conductance.

Gold NRs were synthesized using a non-seeded method.²¹ Briefly, Au (III) chloride trihydrate ($\text{HAuCl}_4 \cdot 3\text{H}_2\text{O}$), silver nitrate (AgNO_3), L-ascorbic acid (AA), and sodium borohydride (NaBH_4) were added to a CTAB solution, which reduced the Au and resulted in NRs. NRs were washed and concentrated by centrifugation (15 min at 10,000 relative centrifugal force (RCF) for a 1.5 mL sample) before being stored in 1 mM CTAB. TEM analysis showed the NRs were $L = 42.1 \pm 9.4$ nm and $W = 12.3 \pm 3.2$ nm (Fig. 1a, Supporting Info).

The CTAB ligand on the NR surface was exchanged with alternative ligands. To replace CTAB with MCA, we used a “round-trip” ligand exchange protocol²⁰ which involves transferring the NRs to an organic phase first, and then back to aqueous phase with the ligand of choice, which was either mercaptohexanoic acid (MHA), mercaptoundecanoic acid (MUDA), or mercaptohexadecanoic acid (MHDA). NR-MHDA were further exchanged with thiolated PEG of three different molecular weights (356, 1000, 5000). NR-MHDA were also subsequently coated with polyelectrolyte monolayers (PEM) alternating between poly(diallyldimethylammonium chloride) (PDADMAC) and poly(styrenesulfonate) (PSS) using a layer-by-layer assembly procedure.²² UV-vis absorption spectra showed that the LSPR did not significantly broaden or shift after the ligand exchanges (Fig. 1b-d), indicating that the NR lattice was unaffected. TEM of NRs before and after ligand exchange also confirmed no change in NR size (Supporting Info). Previously, we demonstrated that this ligand exchange method results in a uniform NR charge distribution as evidence by gel electrophoretic mobility.²⁰ We assume that the surfaces are saturated by the exchanged ligand, but this is an assumption.

Electrophoretic mobility is sensitive to the effective hydrodynamic radius of a particle, R_{eff} , and thus also to ligand thickness. Mobility shifts in gel electrophoresis show expected trends with ligand chemistry (Fig 2a). MCA coated NRs exhibit shifts to lower mobility with increasing carbon chain length due to slight increases in R_{eff} (Fig 2a, lanes 3-7). Also, LSPR peaks of the MCA coated NRs showed expected shifts with increasing chain length, due to the change in the index of refraction with ligand length²⁰ (Fig 1c).

PEG-SH coated NRs exhibit shifts to lower mobility with increasing PEG chain length (Fig. 2a, lanes 1-2, NR-PEG₅₀₀₀ runs so slowly under these gel conditions it was not included in the analysis). LSPR peaks do not shift with PEG functionalization (Fig. 1b), similar to previously obtained results.²⁰

Layer-by-layer coated NRs exhibit behavior that is consistent with deposition of PEMs. Gel electrophoresis showed alternating charge that matched the charge of the outer most PEM on the surface (Fig. 2a, lanes 7-8). NR-MHDA is 0 layers, and positively charged NRs aggregate in running buffer and

do not migrate in gels, so these were omitted from gel analysis. LSPR peaks blue shift slightly for positively charged and red shift slightly for negatively charged outer most PEM (Fig. 1d).

We used Ferguson plot analysis of gel electrophoresis data to determine the effective hydrodynamic radius (R_{eff}) of the NRs coated with the different ligands.^{23, 24} NR mobility, M , was calculated by dividing the band position in the gel (cm) by the time (s) and strength of the applied electric field (V/m). $\log(M)$ was plotted against gel percentage, $T = 0.75 - 2.0 \%$, for each sample (Fig. 2b). R_{eff} was obtained from the slope of the Ferguson plots using well-established equations relating M and R_{eff} .²⁴ Size standards were run in the gel to obtain the relationship between slope and R_{eff} (Supporting Info). Since the NRs are not spherical, the obtained R_{eff} needed to be converted to length and diameter. The mobility of a particle through the gel is dominated by the particle surface area,^{25, 26} so to convert from R_{eff} to ligand layer thickness, t_{lig} , we assumed surface area conservation:

$$4\pi R_{eff}^2 = 2\pi \left[(r_{NR} + t_{lig}) l_{NR} - 2r_{NR} \right] + 2(r_{NR} + t_{lig})^2 \quad (1)$$

where l_{NR} and r_{NR} are the mean NR length and radius, as determined by TEM. For NR-MCA, t_{lig} obtained from Ferguson analysis increases ~ 3 nm with increasing chain length, similar to values for alkanethiols on gold surfaces (Fig. 2c).²⁷⁻²⁹ t_{lig} increases ~ 2 nm with increasing PEG MW for the NR-PEG, and ~ 4 nm with the addition of two polyelectrolyte layers on the NR-MHDA.

Transient absorption (TA) spectroscopy was used to measure thermal dissipation from the NRs upon photoexcitation.^{19, 27-29} Briefly, a 400 nm, 100 fs, 75 $\mu\text{J}/\text{cm}^2$ laser pump pulse was used to excite the NRs. The fluence of this laser is well below the threshold corresponding to the onset of melting of 220 $\mu\text{J}/\text{cm}^2$.¹² Following this, a probe pulse at 800 nm was used to measure the absorption as a function of delay time.^{13, 30} Because the probe pulse is to the red of the LSPR peak where the absorption spectrum is steep, (Fig. 1b-d), small changes in LSPR position resulted in relatively large changes in the TA signal.

Immediately after pump laser excitation, the LSPR shifts due to a combination of the extension and breathing vibrational modes and thermal expansion.¹⁸ The vibrational modes dominate the shift in the LSPR peak and result in oscillations in the TA signal for $t < 300$ ps (the vibration regime). The TA

signal for NRs coated with MHA is clearly different than the MUDA or MHDA-NRs in the vibration regime, an observation similar to previous experiments where free CTAB concentration was varied about CTAB's cmc (Fig. 3a).¹³ Once these vibrational modes dissipate at ~ 300 ps, the TA signal is dominated by thermal expansion (the diffusion regime). For the small NR temperature rises in these data, the TA signal in the diffusion regime is linearly proportional to the temperature rise of the NRs.¹⁷

To calculate the effective thermal interface conductance of the ligand, G , we fit the TA signal in the diffusion regime ($t > 300$ ps) to the temperature predicted by a finite element numerical model for transient heat conduction from the NR to the surrounding liquid. Using COMSOL Script (www.comsol.com), we performed least squared error regressions to fit the data (dots, Figs. 3b-d) to the model (lines, Figs. 3B-d) to determine G (see Supporting Info. for more details). Since this approach accounts for the thermal mass of the ligand layer, it requires t_{lig} obtained from the Ferguson analysis above. The thermal conductance of the ligand layer is lumped together with the NR-ligand and ligand-fluid thermal interface conductances into the one parameter, G .

Obtained G values for the different ligand chemistries are shown in Table 1. We found that for MHA $G = \infty$ MW/(m² K), for MUDA $G = 175 \pm 75$ MW/(m² K), and for MHDA $G = 163 \pm 35$ MW/(m² K). For all of the thicknesses of the thiolated PEG and polyelectrolyte layers (TA data, Supporting Info.) $G = \infty$ MW/(m² K).

When comparing G values for the three lengths of MCA, we find that if the carbon chain is long enough, G is independent of ligand length. Values are similar to those reported for CTAB coated NRs if the NRs are in a CTAB solution above the CTAB cmc.¹³ Previously reported values for G for Pt and AuPd spherical nanoparticles stabilized by thioalkylated ethylene glycol, tiopronin, and CTAB in aqueous solution range from 145 - 250 MW/(m² K).¹⁷ Wang et al.^{31,32} used vibrational sum-frequency generation (SFG) spectroscopy to investigate the molecular effect of heating an alkyl chain. Mercaptoalkanethiolates on planar gold surfaces had $G = 220 \pm 100$ MW/(m² K), which was independent of chain length. By measuring the time between the pump pulse and heat detection at the terminal methyl group as a function of alkyl chain length, they determined that heat propagates

ballistically along the chains at a velocity of 0.95 nm/ps. By extrapolating to $t = 0$, the initial step in the heat transfer from the Au to the alkyl chain is of length equal to 4 - 5 carbon segments. This is in agreement with data indicating that phonons delocalize over 4 - 5 carbon segments.³¹⁻³³ MHA has only 5 carbons before the terminal carboxyl group, so phonons leaving the NR directly couple with the solvent, thus an infinite G is to be expected. We also found that G approaches infinity and is independent of PEG length and numbers of layers of polyelectrolyte. When comparing G for each ligand type (CTAB vs. MCA vs. polyelectrolyte vs. PEG), we find that G depends on surface chemistry. Both CTAB and MCA form ordered and well-packed, hydrophobic layers that prevent penetration of water molecules. In contrast, PEG and polyelectrolyte layers are hydrophilic and allow for considerable water impregnation, which has previously been experimentally measured³⁴ and modeled by molecular dynamics simulations.³⁵ When water molecules penetrate a ligand layer, they tend to coordinate closely with the ligand atoms and can adopt an ordered structure.³⁶ This makes phonon transport more efficient than in disordered liquid water. Thus, because of their hydrophilic nature, PEG and polyelectrolyte ligands have G approaching infinity. Additionally, it should be noted that since the PEMs are assembled on a MHDA layer and have a G of infinity, the PEMs evidently disrupt the well-ordered, hydrophobic nature of the MHDA and allow solvent penetration.

These results show that the surface coating ligand on NRs influences heat transfer at the interface of the NR with its surrounding. Changing ligand chemistry changes G from 150 to ∞ MW/(m² K). The ability of a ligand to exclude water from the surface of the NR and prevent direct phonon coupling between the NR and solvent is responsible for the variation in G . This result should be carefully considered when selecting a stabilizing ligand for NRs in targeted heating applications. For example, applications that rely on nanorod melting, such as triggered release, should have ligands with low G values, where heat dissipation would be minimal.

ACKNOWLEDGMENT We thank Kimberlee Collins and Professor Gang Chen in the Mechanical Engineering Department at MIT for use of their pump-probe laser, and the Center for Materials Science and Engineering for TEM facility use. This work was supported by the NSF (DMR 0906838).

SUPPORTING INFORMATION PARAGRAPH.

Supporting Information includes additional TEM images, sizing histograms, Ferguson analysis details with size standards, a detailed description of data analysis, and additional transient absorption data. This material is available free of charge via the Internet at <http://pubs.acs.org>.

FIGURE CAPTIONS.

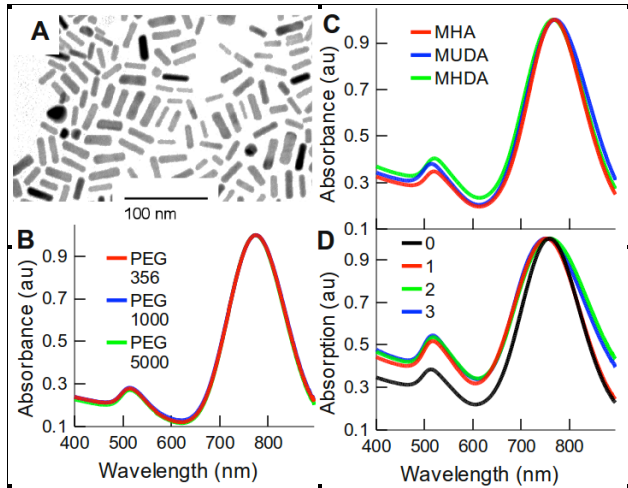


Figure 1. Physical characterization of NRs. a) TEM image of NRs. Optical absorption of b) NR-PEG_{MW} (MW = 356, 1000, 5000). c) NR-MHA, NR-MUDA, and NR-MHDA, and c) NR-MHDA (black) coated with 1, 2, 3 alternating polyelectrolyte layers of PDADMAC and PSS.

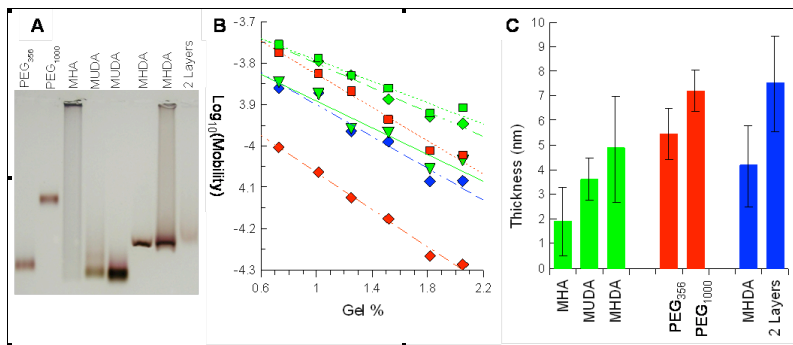


Figure 2. Ferguson plot analysis used to determine the thickness of the ligand layer. a) image of a typical agarose gel used for Ferguson plot analysis. The gel percentage (T) is 0.75 %. The electric field points up in this image, and its strength (E) is 3.9 V/cm. The electric field was on for 2 hours. b) Ferguson plot ($\log(M)$ vs. gel %) of NR-MHA (green squares, dotted line), NR-MUDA (green diamonds, dashed line), NR-MHDA (green down triangles, solid line), NR-PEG₃₅₆ (red squares, dotted line), NR-PEG₁₀₀₀ (red diamonds, dashed line), and NR-MHDA with PDADMAC and PSS (blue diamonds, dashed line). The results of linear regressions used to obtain R_{eff} are shown (lines). c) results of the analysis for ligand thickness, t_{lig} .

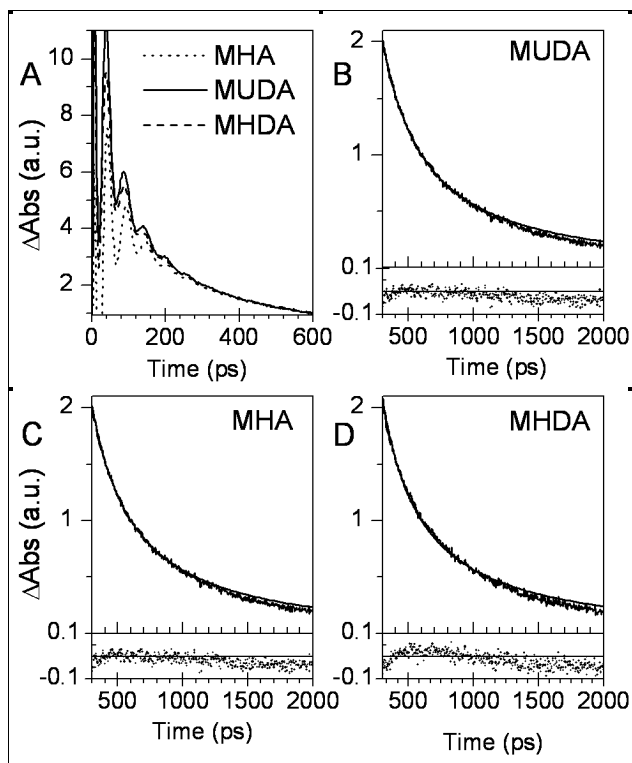


Figure 3. Transient absorption spectra. Entire time length a) NR-MHA, MUDA, and MHDA. Transient diffusion regime: b) MHA, c) MUDA, d) MHDA. Fits: lines. Residuals: below.

TABLES.

Table 1. G values

Ligand	G (MW/m ² K)	R ²
MHA	∞	0.998
MUDA	175 +/- 75	0.992
MHDA	163 +/- 35	0.995
PEG ₃₅₆	∞	0.985
PEG ₁₀₀₀	∞	0.999
PEG ₅₀₀₀	∞	0.999
LbL1	∞	0.998
LbL2	∞	0.994
LbL2	∞	0.978

REFERENCES.

- (1) Niidome, T.; Yamagata, M.; Okamoto, Y.; Akiyama, Y.; Takahashi, H.; Kawano, T.; Katayama, Y.; Niidome, Y., *J. Controlled Release* **2006**, *114*, (3), 343-347.
- (2) Angelatos, A. S.; Radt, B.; Caruso, F., *J. Phys. Chem. B* **2005**, *109*, (7), 3071-3076.
- (3) Hirsch, L. R.; Stafford, R. J.; Bankson, J. A.; Sershen, S. R.; Rivera, B.; Price, R. E.; Hazle, J. D.; Halas, N. J.; West, J. L., *Proc. Nat. Acad. Sci.* **2003**, *100*, (23), 13549-13554.
- (4) Horiguchi, Y.; Niidome, T.; Yamada, S.; Nakashima, N.; Niidome, Y., *Chem. Lett.* **2007**, *36*, (7), 952.
- (5) Kitagawa, R.; Honda, K.; Kawazumi, H.; Niidome, Y.; Nakashima, N.; Yamada, S., *Jpn. J. Appl. Phys* **2008**, *47*, (2), 1374-1376.
- (6) Wijaya, A.; Schaffer, S. B.; Pallares, I. G.; Hamad-Schifferli, K., *ACS Nano* **2009**, *3*, (1), 80-86.
- (7) Agarwal, A.; Huang, S. W.; O'Donnell, M.; Day, K. C.; Day, M.; Kotov, N.; Ashkenazi, S., *J. Appl. Phys.* **2007**, *102*, 064701.
- (8) Huang, X.; El-Sayed, I. H.; Qian, W.; El-Sayed, M. A., *J. Am. Chem. Soc.* **2006**, *128*, (6), 2115-2120.
- (9) Link, S.; El-Sayed, M. A., *J. Phys. Chem. B* **1999**, *103*, (21), 4212-4217.
- (10) Perner, M.; Gresillon, S.; März, J.; von Plessen, G.; Feldmann, J.; Porstendorfer, J.; Berg, K. J.; Berg, G., *Phys. Rev. Lett.* **2000**, *85*, (4), 792.
- (11) Petrova, H.; Juste, J. P.; Pastoriza-Santos, I.; Hartland, G. V.; Liz-Marzan, L. M.; Mulvaney, P., *Phys. Chem. Chem. Phys.* **2006**, *8*, (7), 814-821.
- (12) Alper, J. D.; Crespo, M.; Hamad-Schifferli, K., *J. Phys. Chem. C* **2009**, *115*, (13), 5967-5973.
- (13) Schmidt, A. J.; Alper, J. D.; Chiesa, M.; Chen, G.; Das, S. K.; Hamad-Schifferli, K., *J. Phys. Chem. C* **2008**, *112*, (35), 13320-13323.
- (14) Grubbs, R. B., *Polymer Reviews* **2007**, *47*, (2), 197.
- (15) Sardar, R.; Funston, A. M.; Mulvaney, P.; Murray, R. W., *Langmuir* **2009**, *25*, (24), 13840-13851.
- (16) Selvan, S. T.; Tan, T. T. Y.; Yi, D. K.; Jana, N. R., *Langmuir* **2009**.
- (17) Ge, Z.; Cahill, D. G. B., P. V., *J. Phys. Chem. B* **2004**, *108*, (49), 18870-18875.
- (18) Hartland, G. V., *Phys. Chem. Chem. Phys.* **2004**, *6*, (23), 5263-5274.
- (19) Link, S.; El-Sayed, M. A., *Int. Rev. Phys. Chem.* **2000**, *19*, (3), 409-453.
- (20) Wijaya, A.; Hamad-Schifferli, K., *Langmuir* **2008**, *24*, (18), 9966-9969.
- (21) Jana, N. R., Gram-Scale Synthesis of Soluble, Near-Monodisperse Gold Nanorods and Other Anisotropic Nanoparticles. In 2005; Vol. 1, pp 875-882.
- (22) Gole, A.; Murphy, C. J., *Chem. Mater.* **2005**, *17*, (6), 1325-1330.
- (23) Park, S.; Hamad-Schifferli, K., *J. Phys. Chem. C* **2008**, *112*, (20), 7611-7616.
- (24) Rodbard, D.; Chrambach, A., *Proc. Nat. Acad. Sci.* **1970**, *65*, (4), 970-977.
- (25) Chakraborty, B.; Sha, R.; Seeman, N. C., *Proc. Nat. Acad. Sci.* **2008**, *105*, (45), 17245-17249.
- (26) Rodbard, D.; Chrambach, A., *Anal. Biochem.* **1971**, *40*, (1), 95-134.
- (27) Ehler, T. T.; Malmberg, N.; Noe, L. J., *J. Phys. Chem. B* **1997**, *101*, (8), 1268-1272.
- (28) Sun, Y. G.; Xia, Y. N., *Anal. Chem.* **2002**, *74*, (20), 5297-5305.
- (29) Templeton, A. C.; Pietron, J. J.; Murray, R. W.; Mulvaney, P., *J. Phys. Chem. B* **2000**, *104*, (3), 564-570.
- (30) Schmidt, A.; Chiesa, M.; Chen, X.; Chen, G., *Rev. Sci. Instrum.* **2008**, *79*, (6), 064902.
- (31) Wang, Z.; Cahill, D. G.; Carter, J. A.; Koh, Y. K.; Lagutchev, A.; Seong, N.-H.; Dlott, D. D., *Chem. Phys.* **2008**, *350*, (1-3), 31-44.
- (32) Wang, Z.; Carter, J. A.; Lagutchev, A.; Koh, Y. K.; Seong, N.-H.; Cahill, D. G.; Dlott, D. D., *Science* **2007**, *317*, 787-798.
- (33) Segal, D.; Nitzan, A.; Hanggi, P., *J. Chem. Phys.* **2003**, *119*, (13), 6840-6855.
- (34) Heuberger, M.; Drobek, T.; Voros, J., *Langmuir* **2004**, *20*, (22), 9445-9448.

(35) Kanari, Y.; Shoji, Y.; Ode, H.; Miyake, T.; Tanii, T.; Hoshino, T.; Ohdomari, I., *Jpn. J. Appl. Phys* **2007**, *46*, (9B), 6303-6308.

(36) Kjellander, R.; Florin, E., *J. Chem. Soc., Faraday Trans. 1 F* **1981**, *77*, 2053-2077.

SYNOPSIS TOC.

